Available online at www.sciencedirect.com
ScienceDirect
International Journal of Heat and Fluid Flow 28 (2007) 978–987
International Journal of HEAT AND FLUID FLOW
www.elsevier.com/locate/ijhff

Natural convection in a horizontal fluid layer with a periodic array of internal square cylinders – Need for very large aspect ratio 2D domains

Jae Ryong Lee [a], Man Yeong Ha [a], S. Balachandar [b,*]

[a] School of Mechanical Engineering, Pusan National University, San 30, Chang Jeon Dong, Kum Jeong Gu, Pusan 609-735, Republic of Korea
[b] Department of Theoretical and Applied Mechanics, University of Illinois, Urbana, IL 61801, USA

Received 28 February 2006; received in revised form 13 August 2006; accepted 15 January 2007
Available online 23 March 2007

Abstract

We consider the problem of natural convection in a horizontal layer of fluid, bounded between two infinite parallel plates. The present configuration includes a periodic array of square cylinders embedded within the layer, which introduces an externally imposed horizontal length scale. The central question we address here is the effect of the horizontal extent of the computational domain (and the number of square cylinders contained within the domain) on the flow dynamics and overall heat transfer. Computations that use small aspect ratio domains, which contain only one or two of the square cylinders, severely constrain the plume dynamics. Only large aspect ratio computational domains ($AR \geqslant 10$) allow multiple plumes and their complex dynamics, and begin to approach the results of an infinite layer. Here at a modest Rayleigh number of 10^6, where the flow is unsteady, we systematically vary the horizontal extent of the computational domain by progressively including more of the internal periodic square cylinders. The approach to approximating an infinite layer is observed to be quite slow and even with wide aspect ratio computational domains that include as many as 12 internal periodic square cylinders the asymptotic state is not closely approximated. The need for very large aspect ratio computational domain in such problems is clear.

Keywords: Natural convection; Large aspect ratio; Nusselt number; Periodic boundary condition

1. Introduction

Rayleigh–Bénard convection in a horizontal layer of fluid confined between two infinite parallel plates, with the bottom plate heated and the top plate cooled is well studied for over a century. Numerical models of this problem typically employ a computational domain that is finite along the horizontal directions. In the interest to approximate an infinite horizontal layer of fluid as closely as possible, periodic boundary conditions are applied at the side boundaries. The advantage of periodic boundary conditions over other options is that it preserves the translational invariance of Rayleigh–Bénard convection along the horizontal directions. The horizontal extent of the computational domain, however, introduces an artificial length scale into the problem, whose influence has been the subject of recent investigations (Hartlep et al., 2003; Kenjereš and Hanjalić, 2000; Grossmann and Lohse, 2003).

The aspect ratio (width to height ratio) of the computational domain has no influence in the pure conduction regime. In the convective regime the effect of finite aspect ratio is to quantize the possible wavelengths of the convective roll cells. Thus the choice of aspect ratio has an influence on the onset of convective instability observed in computations. Typically the aspect ratio is chosen to be an integer multiple of the wavelength of the most unstable linear instability mode (Grotzbach, 1983; Sirovich et al., 1989; DeLuca et al., 1990; Christie and Domaradzki, 1993).

Fitzjarrald (1976) performed laboratory experiments of natural convection in an enclosure and considered varying Rayleigh numbers and aspect ratios. The effect of aspect

* Corresponding author. Fax: +352 392 7303.
E-mail address: balals@ufl.edu (S. Balachandar).

0142-727X/$ - see front matter © 2007 Elsevier Inc. All rights reserved.
doi:10.1016/j.ijheatfluidflow.2007.01.005

Nomenclature

L	layer depth	n	distance along normal direction
L_x	horizontal extent of the computational domain	$\mathbf{k}_2$	vertical direction
T_h	hot bottom wall temperature	v	kinematic viscosity
T_c	cold top wall temperature	α	thermal diffusivity
$\mathbf{u}$	nondimensional velocity	g	acceleration due to gravity
θ	nondimensional temperature	β	volume coefficient of expansion
p	nondimensional pressure	Ra	Rayleigh number
t	time	Pr	Prandtl number
t_p	time period of integration	Nu	Nusselt number
U	horizontal velocity	AR	aspect ratio
V	vertical velocity	$\overline{()}$	horizontal-averaged quantity
W	width of the roll cell	$\langle()\rangle$	time-averaged quantity
x, y, z	coordinates		

ratio of the enclosure on the overall Nusselt number was expressed in terms of a correlation. Goldhirsch et al. (1989) numerically investigated the effect of Ra and aspect ratio on the pattern of roll cells formed in the enclosure at Rayleigh numbers higher than criticality. They observed symmetry breaking bifurcation in their flow pattern when the aspect ratio was varied in the range up to four at Rayleigh numbers on the order of 10^4.

Recent simulations of Rayleigh–Bénard convection in a large box of aspect ratio 10 (Hartlep et al., 2003) performed over a range of Rayleigh and Prandtl numbers provide important insight into the appropriate choice of aspect ratio. They showed that large scale roll cells are present even in the turbulent regime and the width of the cells increase from about 2–7 as Ra increased from $O(10^3)$ to $O(10^7)$. The dependence on Prandtl number is quite weak for $Pr < 10$. This suggests the need for a wide aspect ratio computational domain for meaningful higher Rayleigh number simulations. This tendency towards wider roll cells with increasing Ra has also been observed in other studies (Kenjereš and Hanjalić, 2000; Chapman and Proctor, 1980; Hewitt et al., 1980; Ishiwatari et al., 1996; Trompert and Hansen, 1998).

In several practical applications concerning heat transfer by natural convection the geometry of the problem introduces a natural length scale along the horizontal direction. For example, consider the case of convection between infinite parallel plates, but with a periodic array of cylinders embedded within the layer (Ha et al., 2002; Lee et al., 2004a). Here the horizontal spacing between the cylinders introduces a length scale, however, the interest is to approximate an infinite layer consisting of an infinite array of cylinders. Furthermore, continuous translational invariance of the pure Rayleigh–Bénard convection is replaced here by invariance to discrete translations.

Numerical investigations of such problems typically use only a small computational domain limited to a unit cell of the periodic unit containing of only one internal cylinder within the domain (Zhang et al., 1997). Such choice is often justified by the implicit assumption that the geometric periodicity of the problem implies flow periodicity. However, this assumption is not always justified. For example, as seen in Lee et al. (2004a) in the unsteady regime, despite the geometric periodicity, the flow field and temperature distribution are not periodic over a unit cell. The overall heat transfer showed significant fluctuation as the size of the computational domain is varied.

The focus of the present work is to address the fundamental question of how large the computational domain needs to be in order to obtain an acceptable approximation for the infinite layer. Thermal convection in a horizontal fluid layer with internal periodic array of square cylinders is the test bed in which we investigate the effect of computational domain size. We systematically vary the horizontal extent of the computational domain to include from 2 to 12 square cylinders. The results illustrate the importance of using a very wide-aspect ratio computational domain. We believe the observed behavior is applicable to simulations of other similar problems that include geometric periodicity along the horizontal direction.

2. Numerical methodology

The system consists of two parallel horizontal plates separated vertically by height L, between which an array of square solid bodies of size, $L/3$, are centered vertically and equi-spaced horizontally by distance L (see Fig. 1). The bottom wall is kept at a constant high temperature of T_h, whereas the top wall at a constant low temperature of T_c. Along the horizontal direction a periodic boundary condition is enforced. In this study the aspect ratio (width to height) is varied from 2 to 12 and thus the computational domain includes up to 12 square solid bodies within it. The geometry is assumed to be invariant along the z-direction and thus the square bodies represent two-dimensional cylinders of square cross-section. The fluid properties are also assumed to be constant, except for the fluid

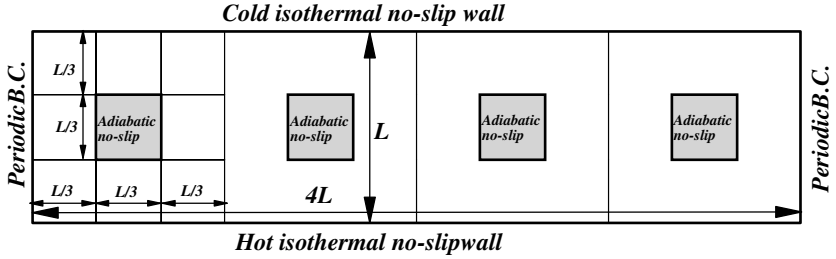

Fig. 1. A schematic of the computational geometry and the boundary conditions for a sample computational domain involving 4 internal cylinders.

density in the buoyancy term, which follows the Boussinesq approximation.

We solve the continuity, Navier–Stokes and energy equations in their nondimensional forms defined as

$$\nabla \cdot \mathbf{u} = 0, \tag{1}$$

$$\frac{\partial \mathbf{u}}{\partial t} + \mathbf{u} \cdot \nabla \mathbf{u} = -\nabla p + Pr\nabla^2 \mathbf{u} + RaPr\theta \mathbf{k}_2, \tag{2}$$

$$\frac{\partial \theta}{\partial t} + \mathbf{u} \cdot \nabla \theta = \nabla^2 \theta, \tag{3}$$

where $\mathbf{u}$, p and θ are the nondimensional velocity, pressure and temperature fields. In the above equations the layer depth (L), α/L and $\Delta T = (T_h - T_c)$ are chosen as the length, velocity and temperature scales. The nondimensionalization results in two-dimensionless parameters: Prandtl number ($Pr = \nu/\alpha$) and Rayleigh number ($Ra = g\beta L^3(T_h - T_c)/(\nu\alpha)$), where ν, α, g and β are the kinematic viscosity, thermal diffusivity, gravitational acceleration and volume expansion coefficient. Here $\mathbf{k}_2$ is unit vector along the vertical direction.

The focus of the present paper is to establish the strong influence of the horizontal extent of the computational domain in the unsteady convection regime. The results to be reported here are for $Ra = 10^6$ and the influence of the computational domain is qualitatively similar at other Rayleigh numbers, where the flow is unsteady. As observed in Lee et al. (2004a), at lower Ra where pure conduction or steady convection prevails, smaller computational domains with periodic boundary conditions are appropriate. In the simulations to be reported here the Prandtl number, Pr, has been taken to be 0.7 corresponding to that of air.

A spectral multi-domain methodology is used for the spatial discretization. Here we employ nine subdomains for each unit aspect ratio of the computational domain. Within each subdomain a local spectral Chebyshev discretization using 31×31 points is defined. For details of numerical methodology, grid independence and other validations using this code and numerical methodology (see Lee et al., 2004a,b; Balachandar and Parker, 2002). The nondimensional time step in these simulations is 10^{-6}. Once the velocity and temperature fields are obtained, the local, surface-averaged, time-averaged, and time-and-surface-averaged Nusselt number are defined as

$$Nu = \left.\frac{\partial \theta}{\partial n}\right|_{\text{wall}}, \quad \overline{Nu} = \frac{1}{L_x}\int_0^{L_x} Nu \, dS,$$

$$\langle Nu \rangle = \frac{1}{t_p}\int_0^{t_p} Nu \, dt, \quad \langle \overline{Nu} \rangle = \frac{1}{t_p}\int_0^{t_p} \overline{Nu} \, dt$$

where n is the normal direction to the walls, L_x is the horizontal extent of the computational domain and t_p is the period of time integration. The above quantities are separately computed for the top cold and the bottom hot walls.

3. Results

The instantaneous thermal fields for the different cases considered with aspect ratio $AR = 2$, 3, 4, 5, 6, 8, 10 and 12 are shown in Fig. 2. The qualitative picture remains the same with one or more upwelling hot plumes, separated by downwelling cold plumes. These ascending and descending plumes drive strong roll cells that extend over the entire depth of the layer. The streamline patterns for the different cases are shown in Fig. 3. The lateral spacing between adjacent plumes thus dictates the horizontal extent of the clockwise and counterclockwise rotating roll cells. The plumes are not evenly spaced and as a result the roll cells vary in size as well. However, the width of all the roll cells must add up to the size of the computational domain. The plumes located at the interface between clockwise and counterclockwise cells of unequal width are typically tilted towards the wider cell. This behavior has been observed in the past (Deardorff and Willis, 1965) and can be explained based on the strength of the adjacent roll cells.

3.1. Average cell width and Nusselt number

The time and surface-averaged Nu measured at the bottom wall is shown in Fig. 4a. The mean Nu shows significant fluctuation as AR is increased from 2 to 12. However, the level of fluctuation decreases with increasing domain size and it appears that it will possibly approach an asymptotic value. The complex up and down behavior seen in Fig. 4a can be explained if we consider the width of the roll cells that can be accommodated within the computational domain for the different aspect ratios. The average width of the roll cells for the different aspect ratio cases is shown in Fig. 4b, where the average is over all the clockwise and counterclockwise rotating roll cells within the

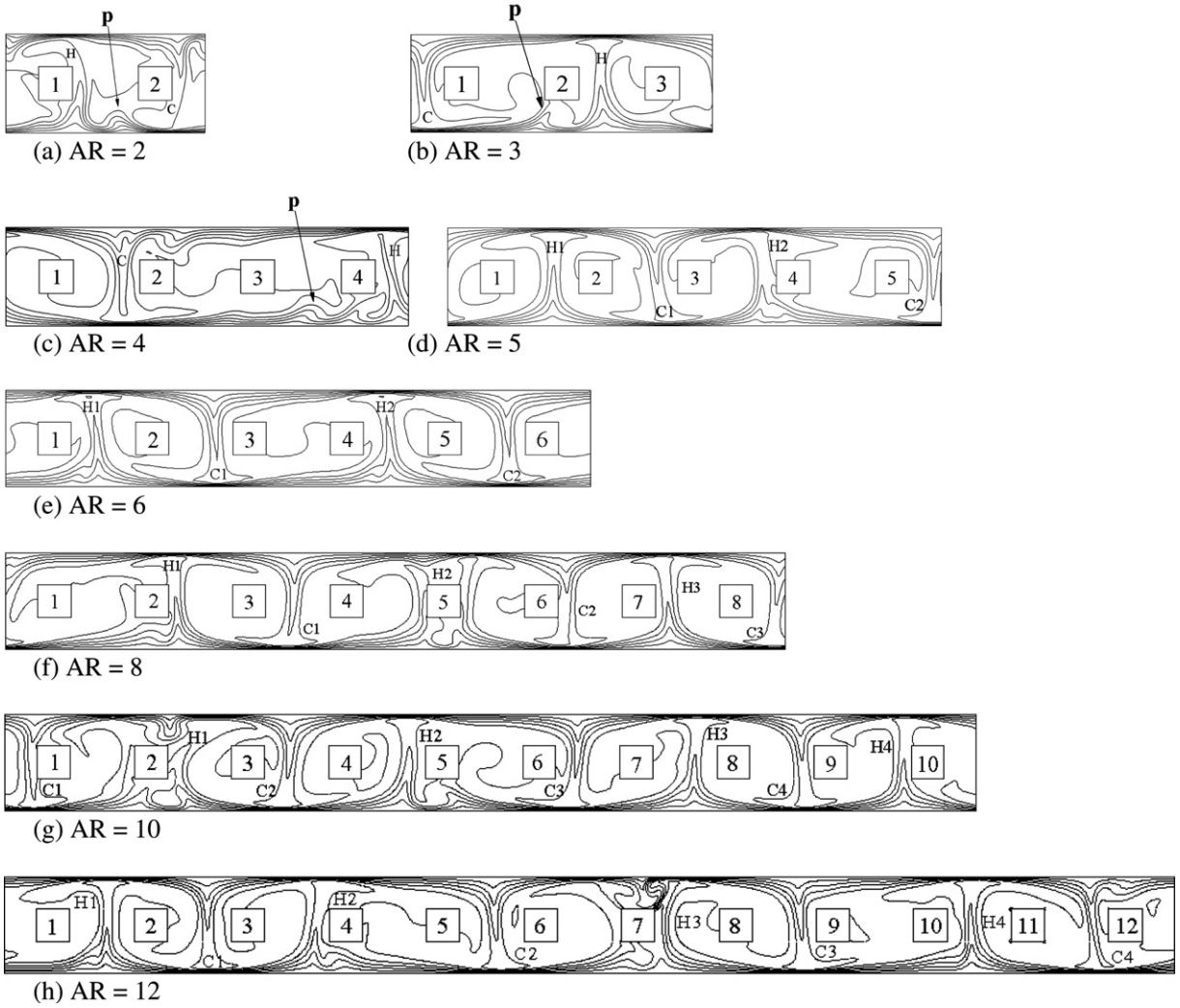

Fig. 2. Instantaneous thermal fields for the different cases considered with aspect ratio $AR = 2$, 3, 4, 5, 6, 8, 10 and 12. The hot upwelling plumes are marked **H1**, **H2**, etc., the cold downwelling plumes are plumes are marked **C1**, **C2**, etc. These flows are strongly time-dependent with small plumelets traveling along the top and bottom boundary layers and merging with the larger plumes. As an example the hot plumelets at the bottom boundary layer are marked as **P** in frames (a), (b) and (c).

computational domain. Note that due to periodic boundary condition along the spanwise direction the roll cells appear as clockwise and counterclockwise pairs and furthermore they are quantized as one, two, three, or four pairs. In case of $AR = 2$, 3 and 4 only one pair of roll cells is observed. As the computational domain expands to $AR = 5$ and 6, two pairs of roll cells are accommodated. For the case of $AR = 8$ we observe three pairs of roll cells and in case of $AR = 10$ and 12 four pairs are observed.

In case of $AR = 2$, the pair of clockwise and counterclockwise roll cells occupy the entire width of the computational domain at all times and as a result the average width of a roll cell is simply 1.0. For the $AR = 3$ and 4 cases, the pair of clockwise and counterclockwise roll cells occupy the entire width of the increasingly wider computational domain and as a result the average cell width increases to 1.5 and 2.0, respectively. With two pairs of roll cells within the computational domain $AR = 5$ and 6 cases result in average cell width of $5/4 = 1.25$ and $6/4 = 1.5$, respectively. In a similar manner the average cell width for $AR = 8$, 10 and 12 can be evaluated as $8/6 = 1.333$, $10/8 = 1.25$ and $12/8 = 1.5$, respectively. In general, as the size of the computational domain is increased we observe the roll cells to expand horizontally and their width to increase (marked **e** in Fig. 4). Every now and then this trend is interrupted when a split occurs and the number of roll cell pairs within the computational domain makes a quantum jump (marked **s** in Fig. 4). This jump is accompanied by a discrete reduction in the average cell width. Thus, the widening of the roll cells, with frequent splitting to form an additional pair of roll cells, results in a complex up and down behavior for the average cell width.

The observed up and down trend in average width vs AR qualitatively mirrors the behavior of mean Nusselt number, $\langle \overline{Nu} \rangle$. In other words, as the mean width of the roll cell increases we observe $\langle \overline{Nu} \rangle$ to decrease and vice versa. The up and down oscillation of $\langle \overline{Nu} \rangle$ is thus a direct consequence of the repeated increase and decrease of the mean

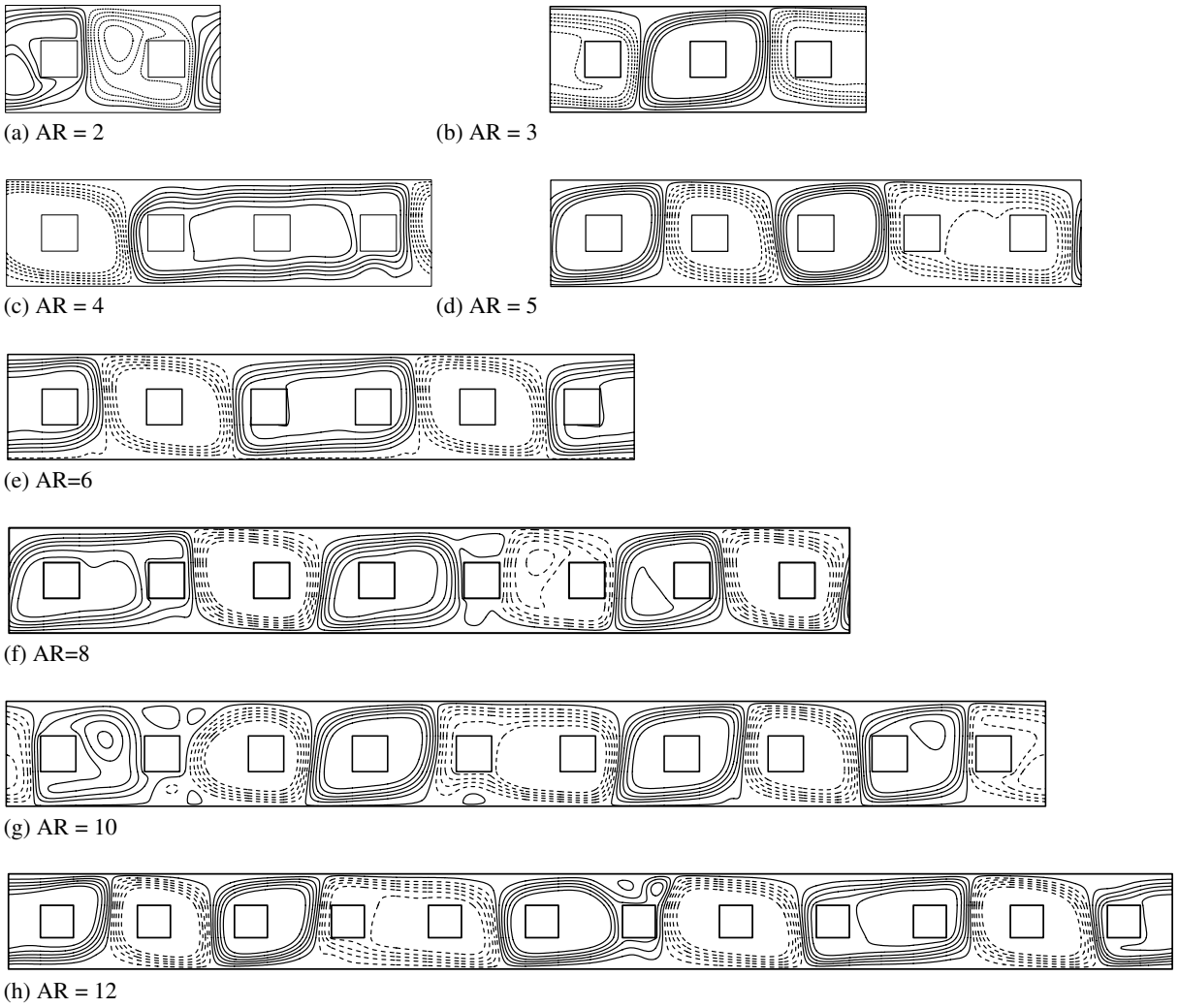

Fig. 3. Instantaneous streamlines for the $AR = 2$, 3, 4, 5, 6, 8, 10 and 12. The time instances shown correspond to those shown in Fig. 2 in order to facilitate direct connection between the thermal and flow fields. It can be seen that the localized recirculations, for example below cylinders 2 and 5, correspond to the plumelets.

cell width. From simple consideration of continuity, the scale of horizontal to vertical velocity of a roll cell can be estimated as $(U/V) \propto (W/L)$, where W is the average width of the roll cell. The relative intensity of horizontal motion linearly scales with the width of the roll cell. As a result, dissipation at the top and bottom boundaries can be expected to be higher for wider cells than for narrower cells. The balance between buoyancy and dissipation thus dictates the intensity of the roll cells (V) to be weaker for wider roll cells and explains the inverse relation between the mean width of the roll cell and $\langle \overline{Nu} \rangle$.

For all the cases considered the flow is highly time dependent and the isotherms shown in Fig. 2 and the corresponding streamlines shown in Fig. 3 are at an instant in time. The hot and cold plumes seen in Fig. 2 move around, but in all cases except $AR = 2$ the plume motion is limited to chaotic back and forth motion across an internal square cylinder. Over the entire length of time integration, for all the cases considered the total number of plumes remains fixed. As a result, although the width of the individual roll cells vary somewhat over time, the total number of roll cells remains stable for the entire duration of time integration and thus for each aspect ratio considered the average width of the roll cell remains fixed.

Note that since the number of roll cells that can fit inside the computational domain is quantized, the average cell width is also quantized. In Fig. 4b, the cross marks present other possible values of average cell width, which the system did not prefer. For example, in case of $AR = 5$, the average cell width for one, two, three and four pairs of roll cells are $5/2 = 2.5$, $5/4 = 1.25$, $5/6 = 0.833$ and $5/8 = 0.625$, respectively. Of which the system chose an average cell width of 1.25. It appears that among the many possible outcomes the system prefers a solution where the average cell width is closest to the asymptotic value corresponding to an infinitely wide layer.

The results presented in Fig. 4b can be used to bracket the average cell width. The result for $AR = 2$ indicates that an average cell width of 0.5 is too small and the system prefers wider cells. Thus, the $AR = 2$ case can be seen to set the

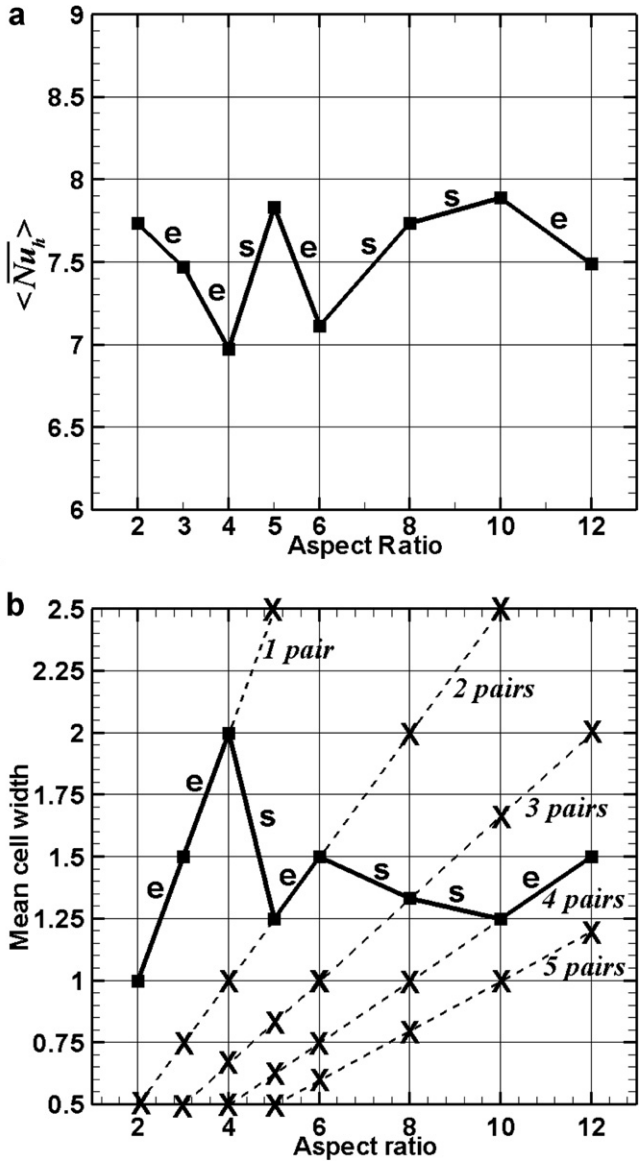

Fig. 4. (a) Time- and surface-averaged Nusselt number and (b) mean width of the roll cells within the computational domain for the different aspect ratio domain. Here **e** indicates when the numbers of roll cells within the computational domains the same but it expands in size, while **s** indicate phase when the number of cells subdivide and as a result their width reduces.

following lower limit for cell width: $W/L > 0.5$. The $AR = 3$ and $AR = 4$ cases progressively increase this lower bound to 0.75 and 1.0, respectively. Note that the bounds set in the lower aspect ratio simulations are not violated as the domain size is increased. For example, for all cases of $AR > 4$, the chosen average cell width is never less than 1.0. Simulations of larger computational domain only tighten the bounds set at smaller computational domains. At $AR = 5$ it is observed that an average cell width of 2.5 is too large and a cell width of 0.833 is tool small and the preferred average cell width is 1.25. Thus an upper bound of 2.5 is introduced, but the lower bound of 1.0 obtained for the $AR = 4$ case is tighter and as a result we obtain $2.5 > W/L > 1$. With simulations of increasingly larger domain we can tighten the upper and lower bounds on the average cell width. From the $AR = 10$ case we obtained an upper bound of $10/6 = 1.666$ and from the $AR = 12$ case we obtain a lower bound of $12/10 = 1.2$ and together from all the cases considered we could place the following bounds for the average cell width: $1.666 > W/L > 1.2$. Note that with simulations on even larger computational domains these bounds can be further tightened. However, the upper and lower bounds approach the asymptotic value rather slowly.

3.2. Unsteady dynamics and heat transfer

The time history of Nusselt number averaged over the bottom plate, $\overline{Nu}$, is shown in Fig. 5 for the eight different cases considered. A remarkable variety of time histories are displayed as the aspect ratio is increased. Due to the symmetry in the problem, the behavior of surface-averaged Nusselt number at the top wall is identical and therefore will not be discussed. The duration time integration typically extends to one viscous time unit, defined as L^2/α. However, at the present Rayleigh number the flow is convection dominated and the duration of time integration covers O(100) plume passages over the internal cylinder, which is in turn related to the time scale on which the roll cells turn over.

The three cases of $AR = 2$, 3 and 4 involve only one of roll cell within the computational domain. However, vastly different Nusselt number behavior is realized emphasizing the importance of the average width of the roll cells in their dynamics. The computational domain of $AR = 2$ is quite confining and results in roll cells of unit aspect ratio. The resulting plume dynamics is unique and quite different from all other cases. Here the Reynolds stress ($\overline{u'v'}$) arising from the tilted plumes drives a mean current (Balachandar et al., 1996). This results in a rapid motion of the bottom boundary layer and the associated hot plume (marked **H** in Fig. 2a) to the right and correspondingly a rapid motion of the top boundary layer and the associated cold plume (marked **C** in Fig. 2a) to the left. During their motion the plumes repeatedly move over the internal square cylinders resulting in a sharp change in instantaneous heat transfer. The plume motion, although by and large repeats, shows subtle chaotic variation and results in a quite complex time evolution of $\overline{Nu}$.

The Nusselt number for the $AR = 3$ case shows both a high frequency and a low frequency component. The higher frequency fluctuations are due to boundary layer instability, which at the bottom wall manifests as small traveling plumelets (marked **P** in Fig. 2b) that merge with the larger hot plume. In this particular case the cold plume (marked **C** in Fig. 2b) periodically moves back and forth to the left and right of the first square cylinder (marked **1** in Fig. 2b), which results in the large amplitude spikes that occur at the low frequency. Only in the $AR = 2$ case the plumes continue to move in one direction. In all other cases the hot and cold plumes are either relatively stationary or

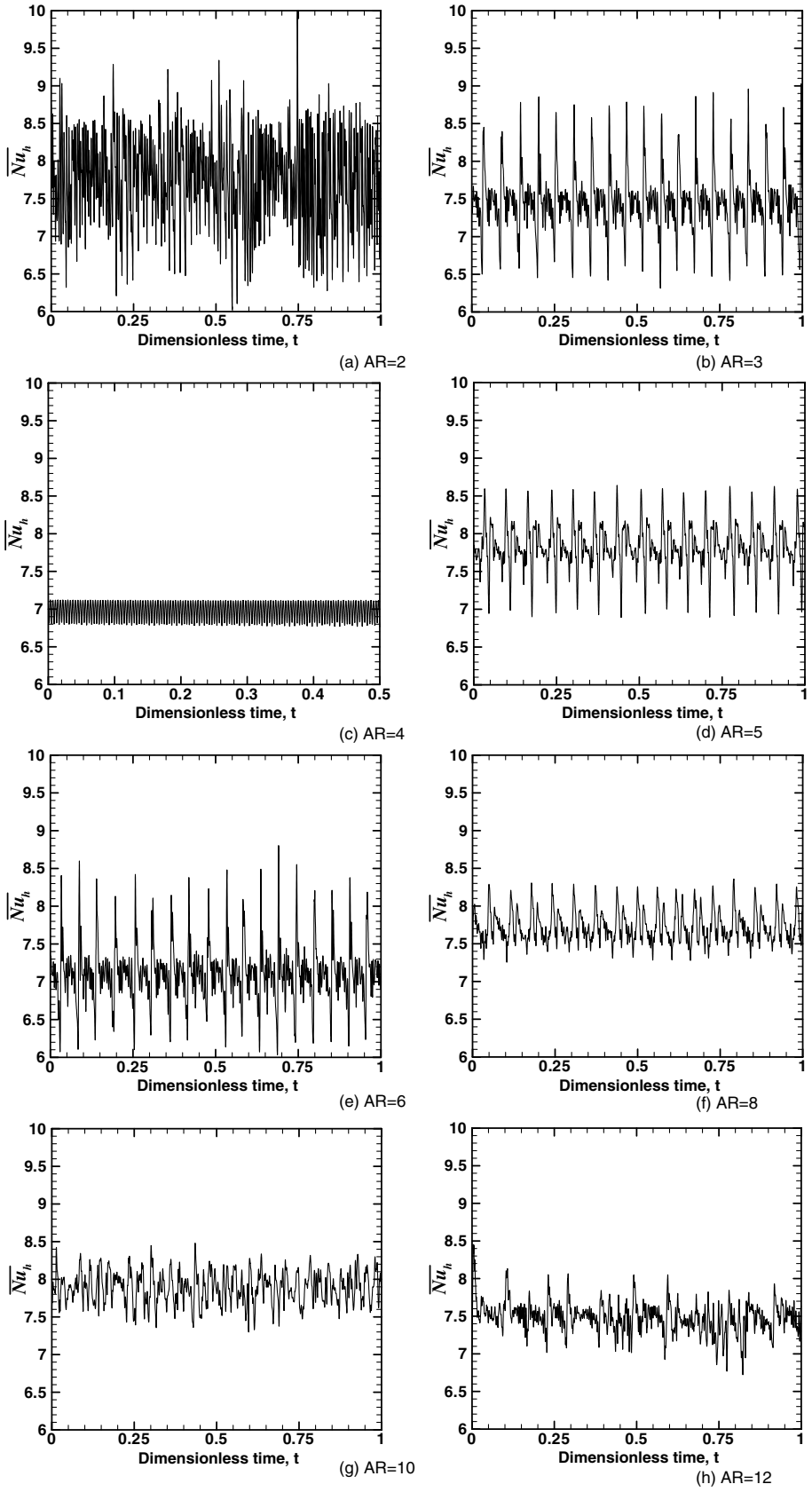

Fig. 5. The time history of Nusselt number averaged over the bottom plate for the eight different cases considered.

at most move back and forth across an internal square cylinder. Accordingly the width of the counterclockwise roll cell changes periodically from 1 to 2 and back, and the width of the clockwise roll cell switches from 2 to 1.

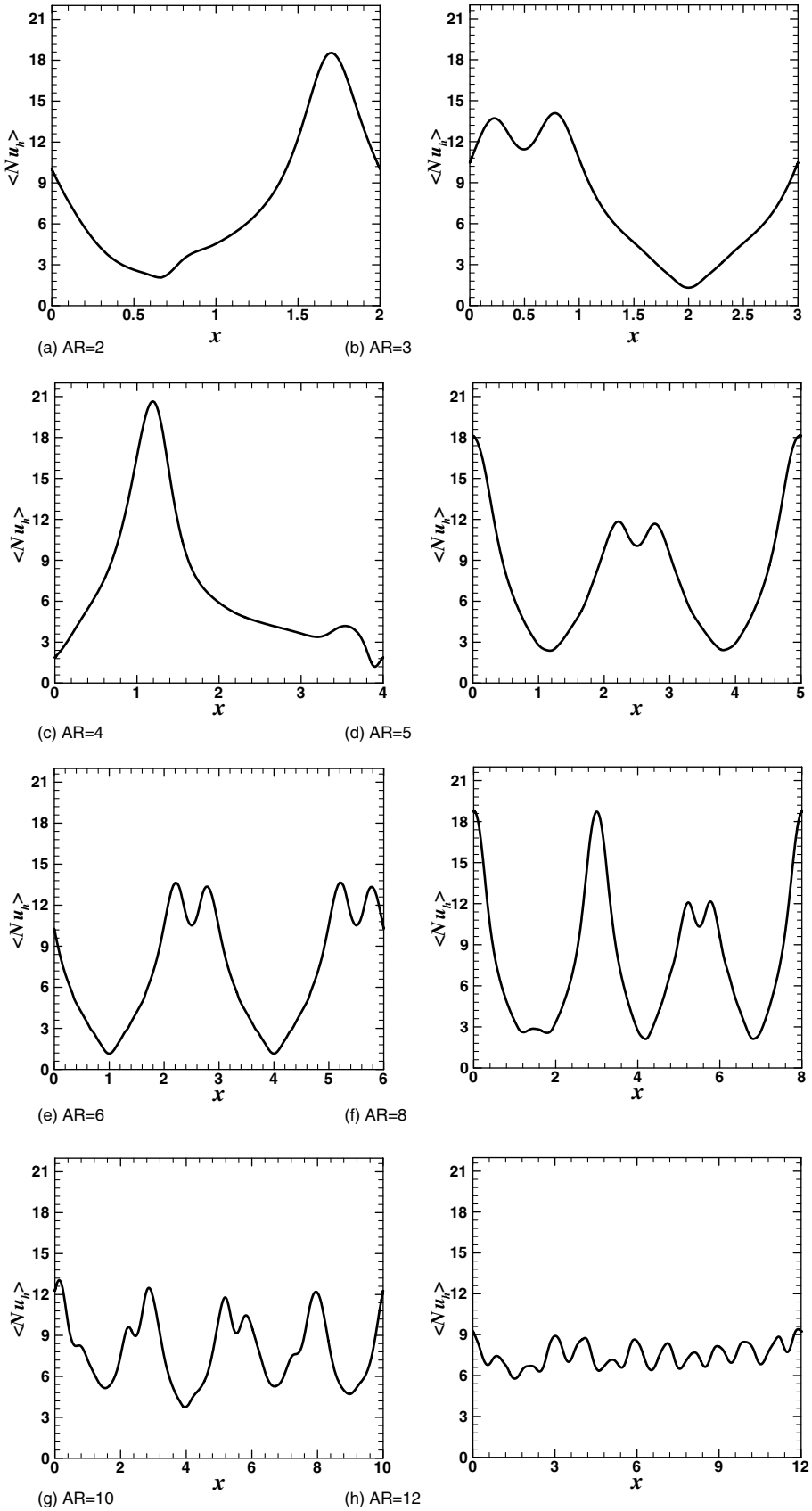

Fig. 6. Time-averaged Nusselt number along the bottom wall for the different cases.

For the $AR = 4$ case the clockwise roll cell is of unit width and the counterclockwise roll cell is of width three. Interestingly the clockwise and counterclockwise rotating roll cells do not want to equi-partition the computational domain into cells of width 2 and 2. For this case both the plumes are relatively fixed in position and do not pass over the internal cylinders and correspondingly the time history of Nusselt number does not show large amplitude low frequency fluctuation. The bottom boundary layers of the wider roll cell undergoes periodic instability with a sequence of small hot plumelets (marked **P** in Fig. 2c) traveling along the bottom wall and merging with the hot plume. These instabilities result in the small amplitude high frequency oscillation seen in Fig. 5c.

When the computational domain is increased to $AR = 5$ the number of roll cells double. At the time instance shown the cell widths are 1, 1, 1, and 2. A movie of the time evolution shows that the central three plumes (marked **H1**, **C1**, and **H2** in Fig. 2d) as a unit move back and forth about the cylinders marked **2**, **3** and **4**. So at other times the roll cell widths are 2, 1, 1 and 1. The high frequency fluctuations in $\overline{Nu}$ are again due to boundary layer instabilities, while the larger amplitude low frequency fluctuations are due to the back and forth oscillation of the plumes. The plume motion and its impact on overall Nusselt number are similar in nature to that seen for the $AR = 3$ case. Two subtle differences can be observed: first, the amplitude of low frequency oscillation is diminished for the $AR = 5$ case. This is due to the fact that the computational domain is now 66% larger than the $AR = 3$ case and thus the impact of an individual cold plume passing over an internal cylinder on the overall heat transfer at the bottom boundary is lower. Second, the frequency of back and forth movement of the plume is 16.7% lower for the $AR = 5$ case.

The Nusselt number evolution for the $AR = 6$ case is qualitatively very similar to the $AR = 3$ case. Instead of one hot and one cold plume we have two hot and two cold plumes. Thus there are two pairs of clockwise and counterclockwise roll cells with each pair behaving similar to the single pair seen in the $AR = 3$ case. If each pair is treated as an oscillator, in this case the two oscillators are synchronized and thus the behavior is virtually similar to that of $AR = 3$.

The $AR = 8$ computational domain allows three pairs of roll cells. While all the plumes show small oscillation in their position only the two left hot plumes (marked **H1** and **H2** in Fig. 2f) move back and forth across internal cylinders marked **2** and **5** to periodically vary the respective cell widths. At the time instance shown we can see the two hot plumes just in the process of moving from the right to the left of the internal cylinder. The motion of the two hot plumes is not perfectly synchronized. Of the three pairs of roll cells one pair is of unit width and it remains this way over the entire duration. In the other two pairs the clockwise and counterclockwise rolls are sometimes of width $(2,1)$ and at other times of width $(1,2)$. The dynamics seen in the $AR = 8$ case appears to be a superposition of dynamics seen for the $AR = 3$ and $AR = 5$ cases.

Both the $AR = 10$ and $AR = 12$ cases have four pairs of roll cells within the computations domain and exhibit fairly complex plume dynamics. As with the $AR = 8$ case, these large aspect ratio cases can also be viewed as a concatenation of smaller units. For example the behavior of the $AR = 10$ case is similar to that of two $AR = 5$ cases. However, if one considers each as a complex oscillator, the combined evolution of two of them is not synchronized. In particular, in these wide aspect ratio domains several plumes move back and forth across internal cylinders resulting in episodic rearrangement of the roll cells. The plume motions are however not synchronized. The interaction between the plumes as they move across the domain is far more complex and the different plumes cross the internal cylinders at different instances in time. As a result the Nusselt number evolution looses the near periodic character seen in the smaller aspect ratio cases. Note the amplitude of these fluctuations is significantly lower due to the wider computational domain. As in the smaller aspect ratio cases there are significant small-scale instabilities of the boundary layers in terms of plumelets, which contribute to the higher frequency component of the surface averaged Nusselt number. The slow approach to an asymptotic state is evident from all the cases presented in Fig. 5.

Time-averaged Nusselt number variation along the bottom wall is shown in Fig. 6 for all the different cases considered. By correlating with the thermal contours in Fig. 2 and streamline pattern in Fig. 3, enhanced local heat transfer can be observed in regions where the cold plume encounters the bottom wall. These are locations where the thermal boundary layer is thinned by the cold downwelling fluid. In contrast, the locations of hot thermal plumes correspond to reduced local heat transfer. As indicated by the plume dynamics, the time-averaged Nusselt number along the bottom wall is not periodic following the geometric pattern. It can be seen that the variation in time-averaged Nusselt number is large at smaller values of aspect ratio and decreases only when AR increases above 10.

4. Conclusion

Here we consider the problem of heat transfer in a horizontal layer of fluid, bounded between two infinite parallel hot bottom and cold top plates that contains a periodic array of square cylinders embedded within it. In this problem the presence of the internal cylinders introduces an external length scale along the horizontal direction. The central question we address here is the effect of the horizontal extent of the computational domain (and the number of square cylinders contained within the domain) on the flow dynamics and overall heat transfer.

As the aspect ratio of the computational domain is increased from 2 to 12 we observe the overall time and area-averaged heat transfer at the bottom wall to suggest a slow nonmonotonic approach to an asymptotic value.

The key feature of the flow is clockwise and counterclockwise rotating pairs of roll cells that are driven by strong upwelling hot and downwelling cold plumes. The finite size of the computational domain places restriction on the possible average width the roll cells can take. Thus, as the aspect ratio of the computational domain is increased we observe the average width of the roll cells to increase if the number of roll cell pairs were to remain the same. But if there is a split and the number of roll cells increase, then the average cell width decreases. There is a direct inverse relation between the average cell width and the overall heat transfer. Thus the up and down behavior of the cell width is responsible for the oscillatory convergence of $\langle \overline{Nu} \rangle$ to an asymptotic state.

The approach to approximating an infinite layer is quite slow. For example, with the present simulations up to an aspect ratio of 12 the mean cell width can be bounded only as follows: $1.666 > W/L > 1.2$. Similarly, one can bound the asymptotic value of time and surface-averaged Nusselt number to be between 7.5 and 7.8. Nevertheless, with a sequence of simulations that includes large aspect ratio domains a clear understanding of the approach to an infinite layer can be obtained.

The time history of surface averaged Nusselt number ($\overline{Nu}$) exhibit a wide variety of behavior as the aspect ratio of the computational domain is increased. The two key controlling features are common in all the cases considered: first, the boundary layer instabilities in the form of plumelets that travel along the surface and merge with the larger plumes are responsible for small amplitude high frequency fluctuation. Second, while some of the large plumes remain relatively fixed in position over the entire duration, other plumes execute a back and forth motion across an internal square cylinder, resulting in a large amplitude low frequency fluctuation in $\overline{Nu}$. Small aspect ratio domains are constraining in terms of possible plume dynamics and results in widely varying $\overline{Nu}$. Large aspect ratio domains ($AR \geqslant 10$) allow complex multiple plume dynamics and as a result only with such large domains asymptotically limiting behavior can be approached. Although the above results are at a single Rayleigh number of $Ra = 10^6$, we believe the qualitative behavior to remain the same at similar Rayleigh numbers where the flow dynamics remains complex and chaotic. The behavior at very high Ra when the flow is highly turbulent is still an open question. Furthermore, the role of three-dimensionality has not been investigated here and its effect can become important at higher Reynolds numbers.

References

Balachandar, S., Parker, S.J., 2002. Onset of vortex shedding in an inline and staggered array of rectangular cylinders. Phys. Fluids 14, 3714–3732.

Balachandar, S., Yuen, D.A., Reuteler, D.M., 1996. High Rayleigh number convection at infinite Prandtl number with temperature-dependent viscosity. Geophys. Astrophys. Fluid Dyn. 83, 79–117.

Chapman, C.J., Proctor, M.R.E., 1980. Nonlinear Rayleigh–Benard convection between poorly conducting boundaries. J. Fluid Mech. 101, 759–782.

Christie, S.L., Domaradzki, J.A., 1993. Numerical evidence for nonuniversality of the soft/hard turbulence classification for thermal convection. Phys. Fluids A 5, 412–421.

Deardorff, J.W., Willis, G.E., 1965. The effect of two-dimensionality on the suppression of turbulence. J. Fluid Mech. 23, 337–353.

DeLuca, E.E., Werne, J., Rosner, R., 1990. Numerical simulations of soft and hard turbulence: I. Preliminary results for two-dimensional convection. Phys. Rev. Lett. 64, 2370–2373.

Fitzjarrald, D.E., 1976. An experimental study of turbulent convection in air. J. Fluid Mech. 73, 693–719.

Goldhirsch, I., Pelz, R.B., Orszag, S.A., 1989. Numerical simulation of thermal convection in a two-dimensional finite box. J. Fluid Mech. 199, 1–28.

Grossmann, S., Lohse, D., 2003. On geometry effects in Rayleigh–Benard convection. J. Fluid. Mech. 486, 105–114.

Grotzbach, G., 1983. Spatial resolution requirements for direct numerical simulation of the Rayleigh–Benard convection. J. Comput. Phys. 49, 241–264.

Ha, M.Y., Kim, I.K., Yoon, H.S., Lee, S., 2002. Unsteady fluid flow and temperature fields in a horizontal enclosure with an adiabatic body. Phys. Fluids 14, 3189–3202.

Hartlep, T., Tilgner, A., Busse, F.H., 2003. Large scale structures in Rayleigh–Bénard convection at high Rayleigh numbers. Phys. Rev. Lett. 91, 064501.

Hewitt, J.M., Mckenzie, D.P., Weiss, N.O., 1980. Earth Planet. Sci. Lett. 51, 370.

Ishiwatari, M., Takehiro, S.I., Hayashi, Y.Y., 1996. The effects of thermal conditions, on the cell sizes of 2-dimensional convection. J. Fluid Mech. 281, 33–50.

Kenjereš, S., Hanjalić, K., 2000. Convective rolls and heat transfer in finite-length Rayleigh–Bénard convection: a two-dimensional numerical study. Phys. Rev. E 62, 7987.

Lee, J.R., Ha, M.Y., Balachandar, S., Yoon, H.S., Lee, S.S., 2004a. Natural convection in a horizontal layer of fluid with a periodic array of square cylinders in the interior. Phys. Fluids 16, 1097–1117.

Lee, D.H., Ha, M.Y., Balachandar, S., Lee, S.S., 2004b. Numerical simulations of flow and heat transfer past a circular cylinder with a periodic array of fins. Phys. Fluids 16, 1273–1286.

Sirovich, L., Balachandar, S., Maxey, M.R., 1989. Simulations of turbulent thermal convection. Phys. Fluids A 1, 1911–1914.

Trompert, R.A., Hansen, U., 1998. On the Rayleigh number dependence of convection with a strongly temperature-dependent viscosity. Phys. Fluids 10, 351–360.

Zhang, L.W., Balachandar, S., Tafti, D.K., Najjar, F.M., 1997. Heat-transfer enhancement in inline and staggered parallel-plate fin heat exchanges. Int. J. Heat Mass Transfer 40, 2307–2325.